WMM'16

CSM
Centro Sviluppo Materiali

7th International Conference
On Magnetism
And Metallurgy

Co-sponsored by:

UK Magnetic Society

Associazione Italiana Metallurgia

Coiltech 2016

WMM'16

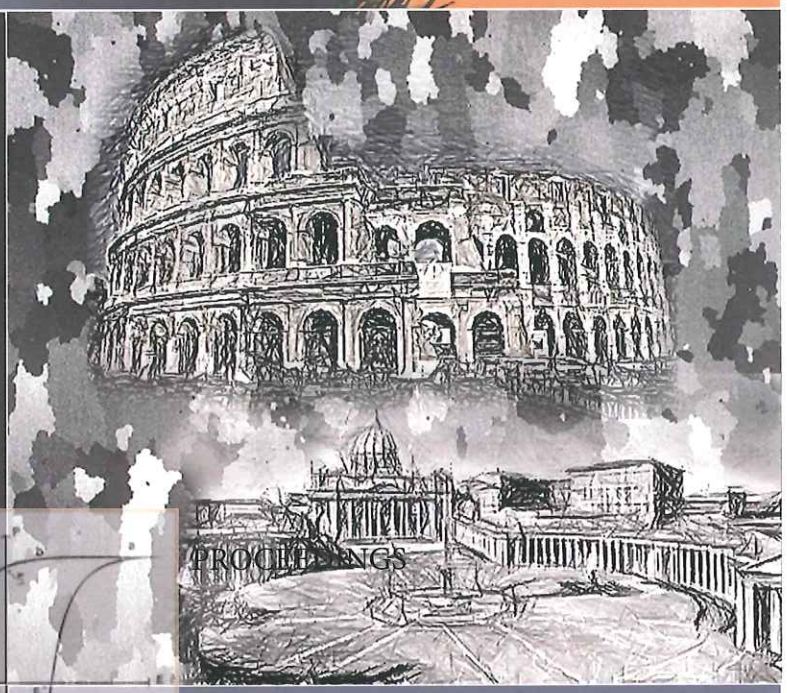

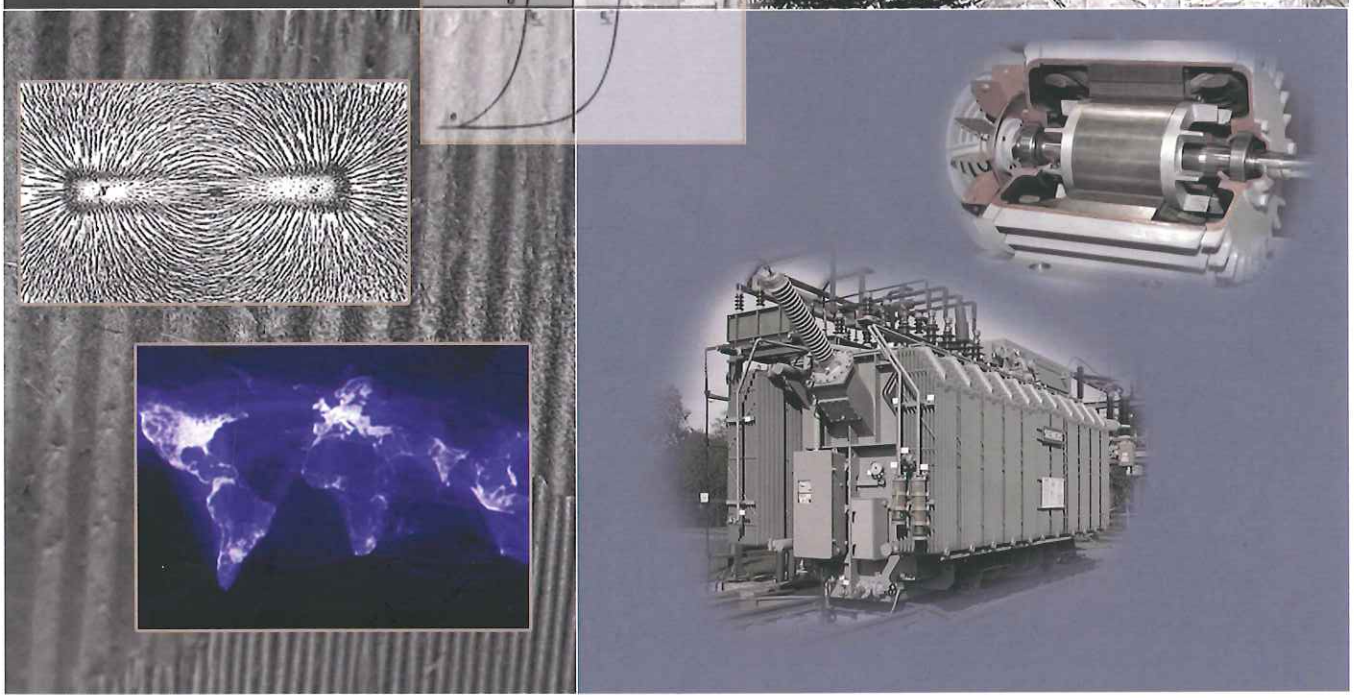

Rome – Italy

June 13 to 15, 2016

PROCEEDINGS

CSM Centro Sviluppo Materiali
materials, technology & innovation

Coiltech 2016
28-29 September Pordenone - Italy

The 7th international Conference on Magnetism and Metallurgy WMM16 takes place in Rome, Italy from June 13th to June 15th (2016) and it is organized by the Centro Sviluppo Materiali - CSM Italy in collaboration with the Department of Industrial and Information Engineering and Economics of University of L'Aquila and the Institute of Metal Forming, Technische Universität Bergakademie of Freiberg. The conference is co-sponsored by the Associazione Italiana Metallurgia – AIM, the UK Magnetic Society and COILTECH - International Coil Winding Expo and Conference

Chair
Manager

R. Kawalla, Freiberg
J. Schneider, Freiberg
Y. Houbaert, Gent

Program

J. Schneider

Local Organizing Committee

Dr S. Fortunati – CSM (Chair)
Prof. M. Villani – University of L`Aquila
Dr E. Amici – CSM
Dr. C. Forzanti – CSM
Dr. S. Cicale' – CSM
Dr. L. Albini – CSM

International Advisory Committee

B. Grieb, Germany
G. H. Johnston, USA
Guo-Dong Wang, China
S. Siebert, Germany
S. Constantinides, USA
S. Fortunati, Italy
G. Pasquarella, Switzerland
A. Krings, Sweden
A. Stöcker, Germany
A. Schoppa, Germany
M. Villani, Italy
F. J.G. Landgraf, Brazil
P. Anderson, UK

These conference proceedings contains the Lectures presented by the Invited Speakers as well as the papers presented in the Poster Session.

Each individual author is responsible for the content of his paper

Publisher : CSM – CENTRO SVILUPPO MATERIALI S.P.A
VIA DI CASTEL ROMANO, 100
00128 - ROME – ITALY
Tel : 0039 – 06 - 50551

Printing : May 31 2016

ISBN : 9788890003301

Requirements on Soft Magnetic Materials for Electric Traction Motors

Andreas Ruf, Simon Steentjes, Georg von Pfingsten, Thorben Grosse, and Kay Hameyer
Institute of Electrical Machines, RWTH Aachen University
Schinkelstr. 4
Aachen, NRW, 52062
Germany

Summary

Electrical traction machines for automotive applications require high power density, high efficiency and high torque, for maximizing the overall performance of the drive train and for minimizing the consumption of energy, i.e., conservation of battery power. Most frequently, permanent magnet synchronous machines with buried magnets that are arranged V-shaped or one above the other (collector arrangement with increased reluctance torque) are the preferred choice for electric and hybrid vehicles. For cost reasons, fault tolerance or certain applications, such as medium- and heavy-duty vehicles, induction machines represent a particularly suited alternative and are the main workhorse. In either case, the utilized electrical steel grade for the lamination stack is critical to the power density, efficiency and torque production, but proper quantification is missing.
The objective of this paper is to elaborate a methodology for selecting the optimal steel grade for the construction of permanent magnetic synchronous and induction machines in due consideration of the application-specific requirements on torque-speed operating points. A material comparison study is presented both for two different permanent magnet synchronous machines as well as an induction machine subject to the same operating requirements in terms of torque and speed, i.e., all have to meet the requirements of the same driving cycle (Worldwide Harmonized Light-Duty Vehicles Test Cycles WLTC Class 1, Class 2 and Class 3). The impact of different electrical steel grades, e.g., sheet thickness and silicon content, on the operational characteristics along the torque-speed map is analyzed numerically using the in-house solver *py*MOOSE. In order to determine the efficiency of each combination of machine topology and lamination type, a transient iron-loss model is used in combination with a machine simulation scheme of the entire operating range of the machine. The notion of steel efficiency is used to compare the different combinations.

I. Introduction

Majority of electric machines for propulsion of electric and hybrid vehicles are speed variable drives. Principal requirements are high power density, high efficiency and high torque at minimal cost. All these are directly related to the material utilization that is strongly dependent on the driving cycle of the machine's application [1, 2]. Op-

timizing the drive for a specific working point is not sufficient on that account [3]. For instance, in order to determine the overall efficiency for an entire driving cycle, all operating points have to be considered including their frequency of occurrence. The rigorous knowledge of the different loss mechanisms, e.g., the iron losses, can enable the possibility to exploit specific loss effects to enhance the drive in particular working points or for specific operational conditions [4, 5]. On the other hand the most appropriate material choice can be realized with this specific knowledge.
Traditionally permanent magnet synchronous machines are applied mainly because of their high efficiency, power density, compactness and zero-speed torque [6, 7, and 8]. Among the alternatives for cost reduction, fault tolerance and lower maintenance, the induction machine has the advantages not to depend on rare earth magnets price, having an increased thermal stability, a very robust design, no induced flux when not excited (in the event of an error) and no need for position decoder [6, 7]. Comparisons have been proposed to indicate the merit of each motor topology for electric and hybrid electric vehicle application [9, 10, and 11]. A comprehensive side-by-side comparison among different traction motor topologies for electric and hybrid electric vehicle applications under consideration of their operating specific requirements (driving cycle) and soft magnetic material utilization is missing.
The very fact that the operating point in speed variable drives changes continuously requires that the machine performance must be studied over the driving cycle of the vehicle instead of in the rated operating point of the machine only.
This paper presents a comparative evaluation of selected motor topologies including two different permanent magnet synchronous machines with interior magnets and one induction machine aiming for a numerical comparison of traction motor performance versus its bill of materials for different choices of electrical steel. The above-mentioned machine requirements (high torque density, high efficiency) have to be satisfied in a wide operational speed range. For a given application this translates on the material level into finding the optimal electrical steel having the best compromise between high polarization and low iron losses. Hence, different electrical steels for the machine's core are analyzed within this study. A numerical comparison study is carried out, aiming to quantify the effect of electrical steel selection on efficiency, torque production and bill of materials: in other words, the added value in terms of motor performance is quantified for different enhanced electrical steel grades. In traction applications, the operating point of the machine changes almost continuously. Therefore, the machine performance is evaluated for all three machine topologies and different electrical steel grades subject to the same operating requirements in terms of torque and speed, i.e., all have to meet the requirements of the same driving cycle (Worldwide Harmonized Light-Duty Vehicles Test Cycles WLTC Class 1, Class 2 and Class 3). For determination of the efficiency of each combination of machine topology and lamination type, a transient iron-loss model is used in combination with a machine simulation scheme of the entire operating range of the machine. This allows to study the impact of different electrical steel grades, e.g., sheet thickness and silicon content, on the operational characteristics along the torque-speed map.

II. Electrical Vehicle and Application Dependent Driving Cycles

In order to evaluate multifarious driving conditions in practice and the demands in terms of torque and speed production on the drive unit, it is prerequisite to establish an entire validation model that includes the vehicle, the motor and a driving cycle.

Appraisal of a single operating point or a few is not sufficient for traction applications where the operating point of the machine changes almost continuously. This model enables characterizing different motor-vehicle combinations subject to different driving cycles. The gear, the inverter and the battery are not considered because the operational characteristics of the motor and the electrical steel grade are analyzed in this paper.

Vehicle Model

A vehicle model is required to generate rotational speed and torque data of the motor according to the velocity versus time curve. Based on the underlying driving cycle, the determination of the requirements for torque and speed is done applying the vehicle model. This model is limited to the longitudinal dynamics specification - the influences of cornering are not considered. (1) and (2) are used to estimate the required power F_{req} depending on the conditions of the driving situation and the vehicles properties.

$$F_{\mathrm{req}}=F_{\mathrm{R}}+F_{\mathrm{L}}+F_{\mathrm{S}}+F_{\mathrm{B}} \tag{1}$$

$$F_{\mathrm{req}} = f_{\mathrm{R}} \cdot F_{\mathrm{Z}} \cdot \cos(\alpha) + c_{\mathrm{W}} \cdot A \cdot \frac{\rho_L}{2} \cdot v^2 + \sin(\alpha) \cdot F_{\mathrm{Z}} + (e_{\mathrm{i}} \cdot m_{\mathrm{L}} + m_{\mathrm{V}}) \cdot a \tag{2}$$

F_{R} is the force that is required to overcome the rolling resistance that is proportional to the gravitational force on the vehicle F_{z} , α is the angle of the inclined road measured from the horizontal and the dimensional coefficient of rolling friction f_{r}. The force to overcome the air drag resistance F_{L} depends on the air drag coefficient c_{W}, the cross sectional area *A*, the speed v of the object relative air and the density of air ρ_L. F_{S} is downhill force to overcome the grade resistance that is proportional to the inclination angle α of the road and the weight force F_{z}. m_{V} and m_{L} are the weight of the vehicle and the load. In combination with the rotational inertia e_{i} and the acceleration of the vehicle a, the force F_{B} that is needed to overcome the acceleration resistance is calculated.

Vehicle Data

The minicar is a vehicle that is comparable to the Volkswagen up! or the Ford Ka. These cars are distinguished primarily by the short overall length and the low weight, so that they can be driven energy-saving in urban areas and parked space-saving. Concerning the air drag coefficient c_{W} and the cross sectional area A there is no significant distinction in comparison to midsize vehicles like the Volkswagen Golf or the Audi A3 (Table 1). Midsize cars have a higher weight than minicars. The demands on a delivery vehicle differ from those to passenger vehicles. In addition to a large maximum load, the cargo space of a transport vehicle should provide a large volume and certain accessibility to the goods in transit. The resulting box shape of the rear of the vehicle leads to the much larger air drag coefficients, a larger reference area and to higher weight.

Vehicle parameters	Minicar vehicle	Midsize vehicle	Delivery vehicle
Tare weight m_{V} [kg]	1100	1300	1200
Maximal load m_{L} [kg]	310/2	500/2	700/2
Air drag coefficient c_{W}	0.30	0.29	0.40
Cross section A [m^2]	2.10	2.20	3.60
Weight distribution (f/b)	45 / 55	55 / 45	50 / 50

Table 1: Characteristics of the Examined Vehicles.

Driving Cycle

A driving cycle specifies the conditions and development of speed used for determination of machine efficiency, i.e., energy consumption, and is a series of data points representing the speed of a vehicle versus time. Driving cycles are predominantly applied to compare the characteristics of different vehicles. Figure 1 and 2 depict the speed versus time curves of the three Worldwide Harmonized Light-Duty Vehicles Test Cycles: WLTC Class 1, Class 2 and Class 3. These will be used in the future within the European Union to compare passenger cars and commercial vehicles regarding their performance and efficiency. The total duration of the WLTC Class 3 in figure 1 is 1800 seconds, whereby the standstill time stipulates 242 seconds. The total distance amounts 23.262 km, the maximum acceleration is 1.6 m/s^2 and the highest speed accounts 131.4 km/h. This cycle is applied for vehicles that exhibit a rated power to weight ratio exceeding the limit of 34 kW/t.

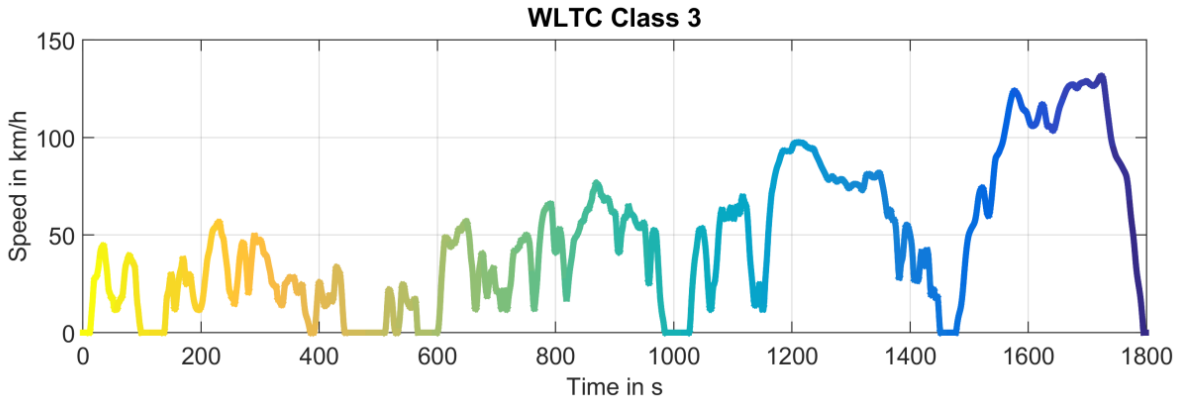

Figure 1.: WLTC 3 driving cycle for vehicles with a power to weight ratio larger than 34 kW/t.

Vehicles that provide a rated power to weight ratio between 22 kW/t and 34 kW/t and additional have a limited maximum speed of 90 km/h are evaluated using the driving cycle depicted in figure 2. Standstill is 223 seconds at a total cycle time of 1477 seconds. The driven distance is 14.664 km, the highest acceleration is 1.0 m/s^2 and the maximum speed is 74.7 km/h.

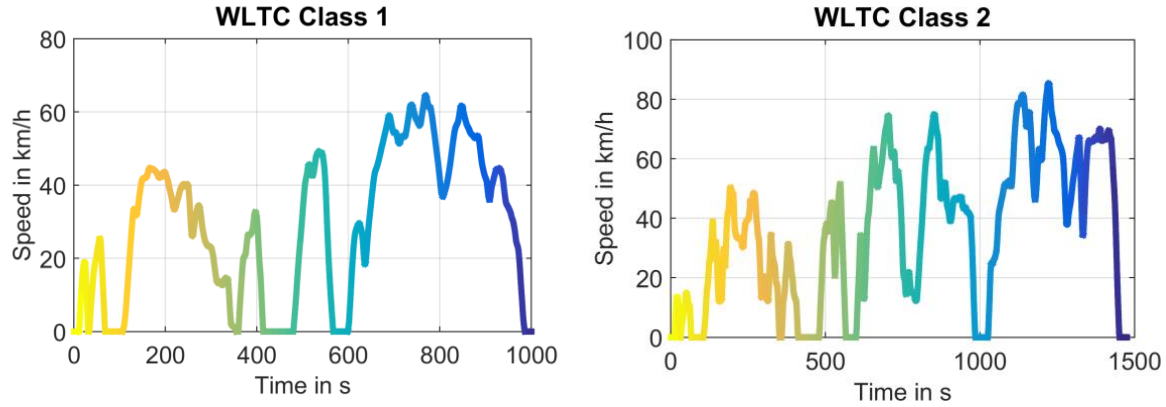

(a) WLTC Class 1 (b) WLTC Class 2

Figure 2.: WLTC driving cycle for vehicles with a power to weight ratio smaller than 34 kW/t.

For vehicles that provide a rated power to weight ratio smaller than 22 kW/t and have a limited maximum speed of 70 km/h, the driving cycle depicted in figure 2 (a) is applied. The standstill time is 203 seconds at a total cycle time of 1022 seconds. The driven distance is 8.091 km, the highest acceleration is 0.8 m / s^2 and the maximum speed is 64.4 km / h.

III. Machine Topologies

The method proposed for the drive cycle analysis is applied to two different permanent magnet synchronous machines and one induction machine designed for a full electric vehicle. Permanent magnet machines have permanent magnets embedded inside the rotor lamination producing negative saliency ($L_\mathrm{q} > L_\mathrm{d}$) enabling the reluctance torque utilization and are the classical solution for electric and hybrid electric vehicles, primarily for light- and medium-duty vehicles. The reason for that is their high efficiency, power density, torque density, compactness and zero-speed torque [6, 7, and 8]. In contrast, induction machines being fully electrically excited have the advantages of lower cost (no permanent magnets), increased thermal stability, fault tolerance (no uncontrolled generation mode), a very robust design and no need for position decoder [6, 7]. Induction machines (IM) have been utilized in electric and hybrid electric vehicles [6-12]. Recently, IMs are used in commercial electric cars such as the Tesla sports car.

Electric Motors

In order to evaluate the proposed methodology, different machine topologies are used that are tailored to different applications subject to application-specific constraints (cost, installation space, overload capability, thermal stability, etc.).
These machines are studied when subjected to the different WLTC driving cycles in order to get a large variety of reliable results. Depending on the performance of the motors listed in table 2 each one of them is employed to another vehicle. Machine 1 (PMSM) is applied to the delivery vehicle, machine 2 (PMSM) to the midsize car and machine 3 (PMSM) drives the minicar vehicle.

Machine Parameters	Machine 1 (PMSM)	Machine 2 (PMSM)	Machine 3 (IM)
Magnet material	NdFeB	NdFeB	-
Number of Poles / Slots $2p$ / N	8 / 48	6 / 36	4 / 36
Winding configuration	Distributed Winding	Distributed Winding	Distributed Winding
Stator radius $r_{\mathrm{stator,o}}$	135 mm	100 mm	87.5 mm
Rotor radius $r_{\mathrm{rotor,o}}$	80 mm	63 mm	51 mm
Axial length active material l_{Fe}	90 mm	80 mm	100 mm
Air gap length δ	0.7 mm	0.75 mm	0.5 mm
Battery voltage U_{dc}	400 V	400 V	130 V
Rated current I_N	142 A	110 A	162.8 A
Rated torque M_{N}	162 Nm	100 Nm	47.5 Nm
Rated speed n_{N}	2500 rpm	2850 rpm	3500 rpm
Rated power P_{N}	42.4 kW	30 kW	17.4 kW

Table 2: Characteristics of the Examined Electric Motors.

The translations of the gear are dimensioned such that every vehicle-motor combination is able to fulfill the requirements set to velocity and acceleration by the WLTC 3 driving cycle. Applying these drive units, consisting of vehicle, motor and gear transmission, to the different WLTC driving cycles generates a wide diversity of operation point distributions and hence, depending on the applied material, various loss characteristics.

IV. Simulation Models

i. Machine Models

For traction drives the induction machine (IM) with squirrel cage rotors and permanent magnet synchronous machines (PMSM) are the most used machine types. Both types of machines do not need slip rings, which decreases the demand of maintenance and the required installation space. As a result both machines have high power densities, which is an imperative need for mobile applications. The IM and the PMSM differ, as their names indicate, in their method of excitation and also in their operational behavior. The PMSM uses magnets for the excitation, which have a fixed installation in the rotor. The excitation field has a fixed position within the rotor, which consequently lead to synchronous operation. The IM utilizes the principle of induction to create an excitation field in the rotor. As the general basis of induction a slip between the rotating field and the rotor is required. It therefore follows a difference in the operational behavior, control and also a difference in the simulation methodology, which needs a brief explanation.
The general intended purpose as a traction drive requires a demand on mechanical power that can be separated in rotational speed and torque. This demand is accomplished by specific control of electrical parameters. The following section introduces a methodology to incorporate the operational characteristics in the simulation of electric machines.

The PMSMs with buried magnets (Table 2) are modeled in a rotor-flux-fixed dq-reference frame including cross coupling magnetization and saturation [13]:

$$\begin{bmatrix}\hat{\psi}_\mathrm{d}\\ \hat{\psi}_\mathrm{q}\end{bmatrix} = \begin{bmatrix}L_\mathrm{dd} & L_\mathrm{dq}\\ L_\mathrm{qd} & L_\mathrm{qq}\end{bmatrix}\begin{bmatrix}\hat{\imath}_\mathrm{d}\\ \hat{\imath}_\mathrm{q}\end{bmatrix} + \begin{bmatrix}\hat{\psi}_\mathrm{f,d}\\ \hat{\psi}_\mathrm{f,q}\end{bmatrix} \tag{3}$$

The quadrature and direct current are varied during simulation to extract the torque calculated by the eggshell method for different excitation [14]. The average torque and the voltage amplitude are determined by the formulas:

$$T = \frac{3}{2}p\left(\hat{\psi}_\mathrm{d}\hat{\imath}_\mathrm{q} - \hat{\psi}_\mathrm{q}\hat{\imath}_\mathrm{d}\right) \tag{4}$$

$$\hat{u} = \omega\sqrt{\hat{\psi}_\mathrm{d}{}^2 + \hat{\psi}_\mathrm{q}{}^2} \tag{5}$$

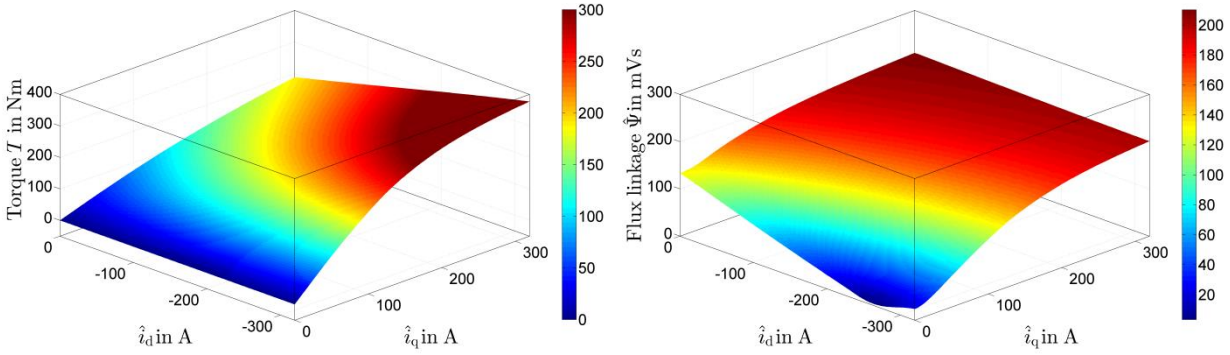

Figure 3: Torque (left) and flux-linkage (right) in dq-reference frame for different current excitations.

Figure 3 shows the result of the calculated average torque and flux-linkage for different dq-current excitations using Finite-Element (FE) simulation. In the case of a PMSM with buried magnets it is shown that the torque and the flux is strongly dependent on the amplitude and angle of the rotor-flux-fixed current vector.

In order to calculate the operating points for the whole operating range, a combined control strategy is used. The optimization problem is defined by:

$$\min_{\hat{\imath}_{\mathrm{d,i,j}},\hat{\imath}_{q,i,j}\in\mathbb{R}} \quad J\left(\hat{\imath}_{\mathrm{d,i,j}},\hat{\imath}_{q,i,j}\right)=\sqrt{{\hat{\imath}_{\mathrm{d,i,j}}}^2+{\hat{\imath}_{\mathrm{q,i,j}}}^2} \tag{5}$$

$$\text{subject to} \quad T_i=\frac{3}{2}p\left(\hat{\psi}_{\mathrm{d,i}}\hat{\imath}_{\mathrm{q,i}}-\hat{\psi}_{\mathrm{q,i}}\hat{\imath}_{\mathrm{d,i}}\right) \quad ,\forall\,\mathrm{i}=1,\dots,\mathrm{m}. \tag{6}$$

$$\hat{u}_{\mathrm{j}}=\omega_{\mathrm{j}}\sqrt{{\hat{\psi}_{\mathrm{d,i}}}^2+{\hat{\psi}_{\mathrm{q,i}}}^2}\leq\hat{u}_{\max} \quad ,\forall\,\mathrm{j}=1,\dots,\mathrm{n}. \tag{7}$$

with the torque vector $T_1,T_2,\dots,T_{\mathrm{m}}$ subject to $\mathrm{m}\in\mathbb{N}$ and the speed vector $n_1,n_2,\dots,n_{\mathrm{n}}$ with $\mathrm{n}\in\mathbb{N}$. This optimization problem combines the maximum torque per ampere (MTPA) control for the base speed range and the maximum torque per voltage (MTPV) control for the field weakening.
Figure 4 shows the trajectories of average electro-magnetic torque calculated with different current excitations. Further an overlapping mesh of calculated operating points using the combined control strategy is mapped. The rotor-flux-fixed current vectors are defined for each operating point by the operating points, which are calculated for the given optimization problem. The basic speed range is represented by the trajectory that extends along the rising torques, whereas the field weakening area is represented by the mesh below this trajectory (Figure 4).

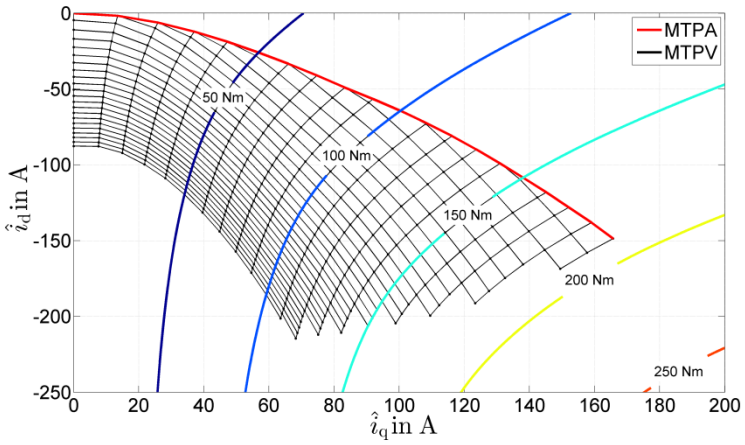

Figure 4: Simulated map of the average torque in Nm with overlapping mesh of operating points.

For the induction machine all reactances and the transformed rotor Ohmic resistance R_2'/s are proportional to the stator frequency ω_1. Therefore the distribution of the stator current I_1 into magnetizing current I_μ and rotor current I_2' can be solely determined by I_1 and slip frequency f_2. This determination is utilized to simulate the operating range of the machines with FE simulations at one synchronous frequency f_1. In the post processing of theses simulations, the voltage is determined by multiplication of the actual synchronous frequency at the desired torque-speed combination with the

value of the simulated stator flux linkage. Field weakening operation is taken into account removing operating points in the $I_1 - f_2$ plane that violate the voltage limit of the inverter. The iron losses are calculated from the local (elementwise) and temporal distribution of the magnetic flux density and is scaled according the synchronous operating frequency. Figure 5 illustrates the operating points of the IM in the torque-speed and the $I_1 - f_2$ plane.

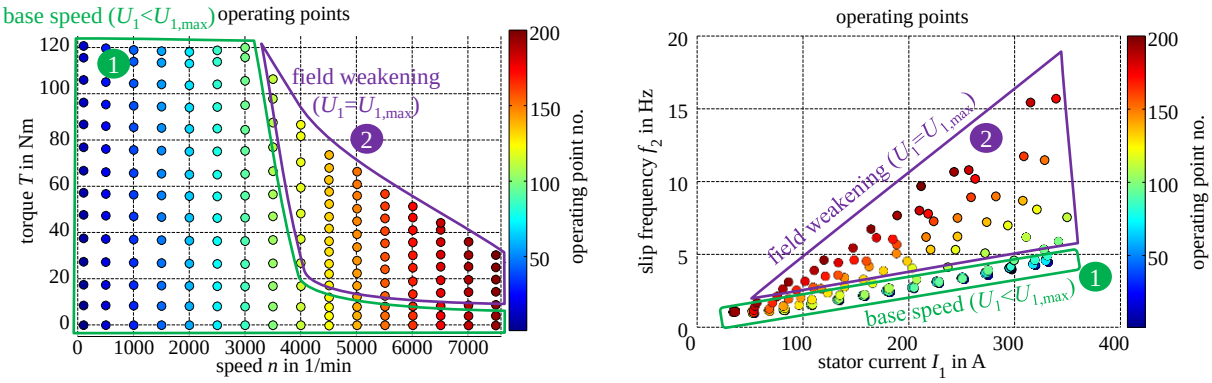

Figure 5: Operating points of the induction machine. In the torque-speed-map (left) and in the stator current-slip frequency-plane (right).

To calculate the efficiency of the different machine toplogies, the various loss components which occur during the operation have to be considered. These are detailed in the following subsections.

i. Ohmic Loss models

The copper or Ohmic losses are calculated according to the following equation:

$$P_{\mathrm{Cu}} = 3R_{\mathrm{S}}(\theta_0)\left(1 + \alpha_{20}(\theta - \theta_0)\right){i_{\mathrm{eff}}}^2. \tag{8}$$

The influence of the changing temperature of the stator windings is taken into account using a temperature dependent stator resistance $R_{\mathrm{S}}(\theta)$. The resistance $R_{\mathrm{S}}(\theta_0)$ is determined by DC measurement at temperature θ_0 and for the simulation results set to a fixed value at temperature $\theta = 100\,℃$ with the temperature coefficient $\alpha_{20} = 3.9 \cdot 10^{-3}\mathrm{K}^{-1}$. For the IM, additionally, the local distribution of the current density in the rotor bar is taken into account, i.e., skin effect especially for bar current temporal harmonics is included in the model.

ii. Iron Loss Models

In order to avoid the disadvantage of high computational effort, it is advantageously to shift from time-harmonic iron loss models to those formulated in the time-domain [15]. In this paper a transient formulation of the iron loss calculation (9) – (12) in the machine is utilized [16] that separates the iron losses in a contribution of hysteresis loss (9), Foucault (macroscopic) eddy current loss (10) and the excess (microscopic) eddy current losses (11). The sum of the three iron loss components gives the total iron losses (12).

$$p_{\mathrm{hy}}(t) = \rho \cdot \left\{ \left| H_{\mathrm{irr}} \frac{\mathrm{d}B_{\mathrm{r}}}{\mathrm{d}t} \right| + \left| H_{\mathrm{irr}} \frac{\mathrm{d}B_{\vartheta}}{\mathrm{d}t} \right| \right\} \tag{9}$$

$$p_{\mathrm{cl}}(t) = k_{\mathrm{cl}} \frac{1}{2\pi^2} \cdot \left\{ \left| \frac{\mathrm{d}B_{\mathrm{r}}}{\mathrm{d}t} \right|^2 + \left| \frac{\mathrm{d}B_{\vartheta}}{\mathrm{d}t} \right|^2 \right\} \tag{10}$$

$$p_{\mathrm{ex}}(t) = k_{\mathrm{ex}} \frac{1}{8.763} \cdot \left\{ \left| \frac{\mathrm{d}B_{\mathrm{r}}}{\mathrm{d}t} \right|^2 + \left| \frac{\mathrm{d}B_{\vartheta}}{\mathrm{d}t} \right|^2 \right\}^{0.75} \tag{11}$$

$$p_{\mathrm{iron}}(t) = p_{\mathrm{hy}}(t) + p_{\mathrm{cl}}(t) + p_{\mathrm{ex}}(t) \tag{12}$$

The hysteresis loss is described by the time differential of the local flux density in radial (B_{r}) and tangential (B_{ϑ}) direction, the irreversible magnetic field strength H_{irr}, and the specific density of the material ρ. The static hysteresis loop is approximated by an equivalent ellipse. From the ellipse formulation, H_{irr} is modeled by the maximum absolute flux density that is reached in the history of the material $\mathrm{B}_{\mathrm{max}}$, the actual absolute value of the flux density B and the hysteresis loss parameter k_{hy}. The iron loss parameter k_{cl} (14) is calculated using the material constants, sheet thickness d, specific electrical resistivity ρ_{e}, and ρ as given in [17].

$$H_{\mathrm{irr}}\left(B, B_{\mathrm{max}}\right) = \frac{k_{\mathrm{hy}} \cdot B_{\mathrm{max}}}{\pi \cdot \rho} \cdot \cos\left(\mathrm{asin}\left(\frac{B}{B_{\mathrm{max}}} \right) \right) \tag{13}$$

$$k_{\mathrm{cl}} = \frac{\pi^2 d^2}{6 \cdot \rho \cdot \rho_{\mathrm{e}}} \tag{14}$$

The values of the loss parameters k_{ex} and k_{hy} are identified using ring cores that are metrological characterized at a Brockhaus MPG 200 measurement system according to the IEC standard (sinusoidal magnetic flux density appraised by form factor deviations). The iron losses are modeled by the time derivative of the flux density (9) – (14). From numerical approximation the iron loss parameters k_{hy} and k_{ex} are found. Fig. 6 shows the modeled and measured iron losses for the material M400-50A and Table 3 gives the identified iron loss parameters of the different electric steel grade.

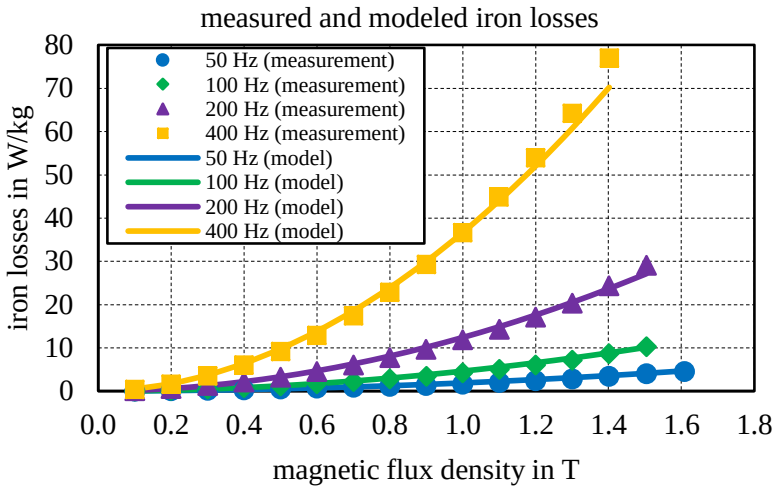

Figure 6: Iron losses from ring core measurements at sinusoidal flux density (points) and from iron loss model (lines).

Material	k_{hy}	k_{cl}	k_{ex}
M250-35A	0.010334	4.49E-05	0.001406
M270-35A	0.015269	5.07E-05	0.000556
M330-35HP	0.020933	6.27E-05	0.000584
M250-50A	0.011184	9.17E-05	0.000828
M400-50A	0.023033	12.7E-05	0.00062
M470-50HP	0.023422	17.8E-05	0.000862

Table 3: Identified loss parameters for different materials.

V. Statistical derivation of magnetic material characteristics

The question of optimal material choice for traction drives used in EV and HEV cannot be solved on basis of standardized material characteristics obtained from Epstein frame, single sheet or ring core measurements only. Steel efficiency is a machine-influencing quantity and it cannot be optimized without consideration of the global efficiency of the motor. The selection of the best material also depends on the typical operational area of the machine [18]. Therefore different publications [1, 3] use driving cycles to evaluate the machine performance considering the operating points. The specific operating points are useful indication values, but still limited with respect on the custom usage of the machine [3]. It is therefore a constrained optimization problem, where the constraint is application and operation dependent, which makes it necessary to incorporate information about the application and statistical aspects of the operation.
In Figure 7 the different driving cycles are applied to the electrical machine (Machine 1) using the presented vehicle model of the delivery van. This example vehicle has to be designed for a maximum Speed of 140 km/h for transportations between different cities (WLTC Class 3). In most cases the vehicle operates in the delivery status within the cities (WLTC Class 1 and 2).

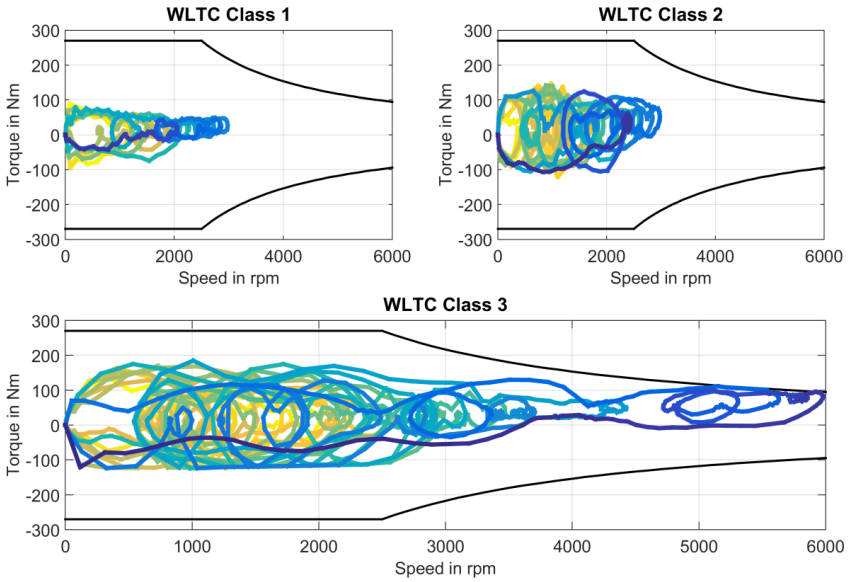

Figure 7: Driving cycles WLTC Class 1-3 applied to a PMSM (machine 1) using a vehicle model.

In order to evaluate the frequency of the applied operational region a bivariate histogram is used. This allows the calculation of the cross probability of torque-speed values. For this operation points, shown in Figure 6, are summed together in discrete operational regions $\left\{\pm 5\,\frac{\mathrm{km}}{\mathrm{h}}, \pm 5\ \mathrm{Nm}\right\}$ to calculate the specific frequency in each region. The gradient between these regions is modeled linearly. The result is the probability $Prob(n, M, \alpha)$ of each operating point of speed n and toque M: (n, M), machine and the holistic characteristic of the machine operation α. Figure 8 presents two representative probability distributions for machine 1.

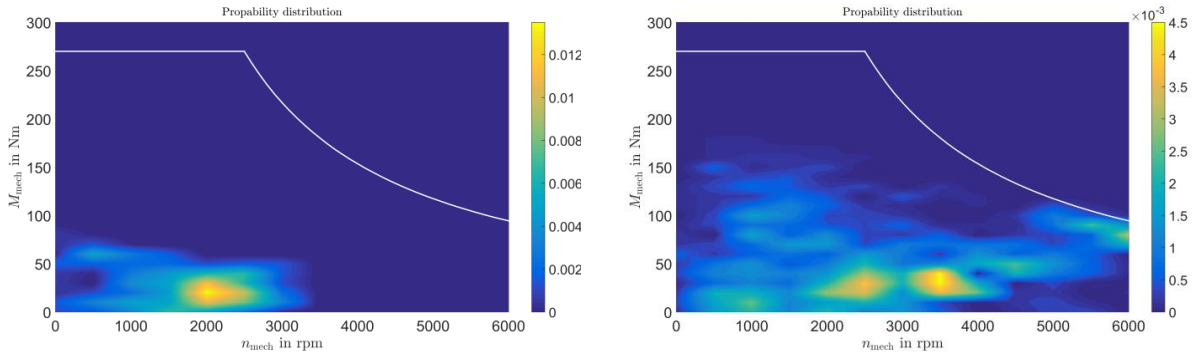

Figure 8: Probability distributions for WLTC Class 1 (left) and WLTC Class 3 (right).

The resulting peaks are typical for driving cycle included speed limits, where the machine has a high probability to be used. These distributions can be used to evaluate the integrated parameters of different steel grades γ. As an example loss components reflect the result of different polarization and loss levels of different materials considering the application usage [2]:

$$P_{\mathrm{Loss}}(\gamma, \alpha) = \int P_{\mathrm{Loss}}(n, M, \gamma) Prob\ (n, M, \alpha)\ \mathrm{d}M\mathrm{d}n \tag{9}$$

Figure 9 depicts exemplary results for machine 1 (PMSM) subject to the driving cycle probability distribution WLTC Class 3 separated in occurring copper and iron loss components:

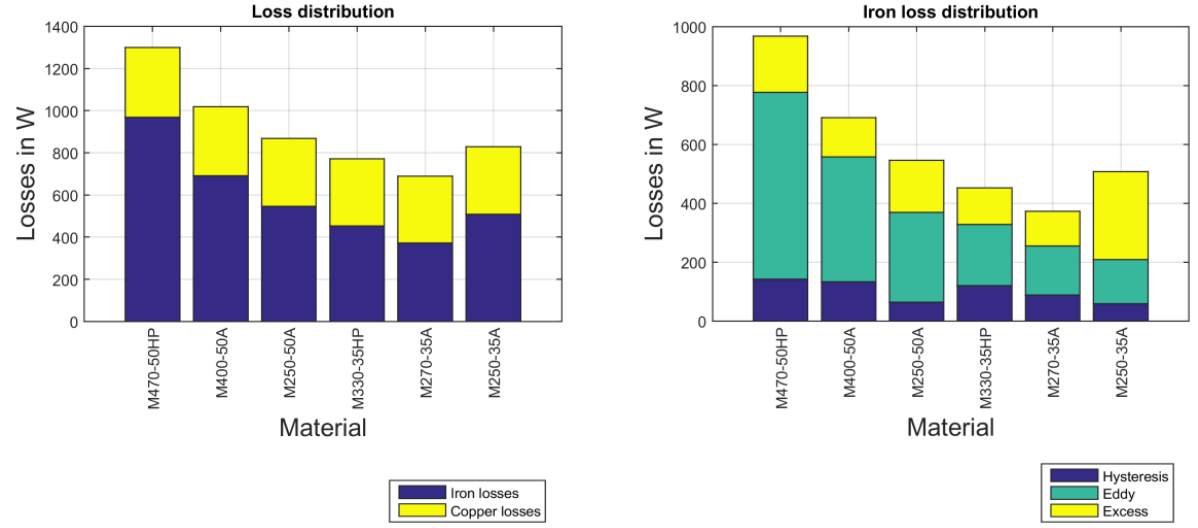

Figure 9: Integrated parameter reflecting the most likely loss components for WLTC Class 3 and machine 1.

As a result this driving cycle distribution includes operation in urban and high speed areas. The probability of high acceleration, e.g., high torques is lower and has a minor effect on the integrated results. Iron losses are the dominant loss component as can be seen in figure 8 (left) for all studied materials. The positive effect of materials with higher polarization is compensated by higher iron losses. The increased iron losses for these materials lead to a load torque which is corrected by the control of the machine and results in higher current demand. This compensating effect leads to copper losses, which are nearly the same. The dominant iron losses add up from different loss components presented in figure 9 (right). For this exemplary driving cycle and application loss components affected by high frequencies are dominant. This result depends on the drive, application and use. This methodology is used to compare different traction drives and applications with different probabilistic calculated parameters in the following section.

VI. Results

The distribution of loss components differs for the particular machine's application and that results in a specific choice of ferromagnetic material. Comparing the different machine topologies and their operation in different driving cycle distributions, it is apparent that the first machine (PMSM) applied in the delivery van (Figure 8 and 9) has a dominant share of iron losses when compared to smaller machines 2 and 3.
According to the standardized measurements the electrical steel grade M250-35A has the lowest sum of iron losses. This is supported by the lowest hysteresis and eddy current loss components. The operation in high frequency ranges contradicts this assumption because of higher excess losses resulting in these operational areas. The electrical steel grades M270-35A and M330-35HP show a better overall performance considering the WLTC 3 operation.
Changing the demand of operation to the WLTC Class 2 (urban) probability distribution decreases the overall iron losses and the relation between iron and copper losses (Fig. 10). M270-35A still delivers the best loss performance, but differences between electrical steel grades decrease. The use of thicker and cheaper materials is an option for this driving cycle. M250-50A delivers approximately the same performance as thinner materials. As a result urban operation decreases the differences between the materials. The benefit of high polarization cannot be exploited by operation in partial load and speed areas, especially when the machine has a higher proportion of iron losses.

The induction machine (machine 3) and the PMSM (machine 2) used in smaller vehicle are designed for the urban and acceleration operation as presented in Figure 11 for machine 2. It can be assumed that materials with higher polarization affect a lower demand on currents to reach higher torques. This should result in lower Ohmic losses and an overall reduction of losses considering the probability distributions for drive cycles. Additionally the relation between iron and copper losses differs to the relation of machine 1 for the delivery vehicle. Figure 12 (left) visualizes the relation between copper an iron losses for the drive cycle in figure 11 (right). The copper losses are dominant and the machine also operates in regions with high torque. The integrated evaluation of loss components shows a maximum change of copper loss parameters of 4.6 % from the best to the worst material. Part of the explanation lies in the fact that a high flux resulting from high polarization is not desired in all operational regions for PMSM.

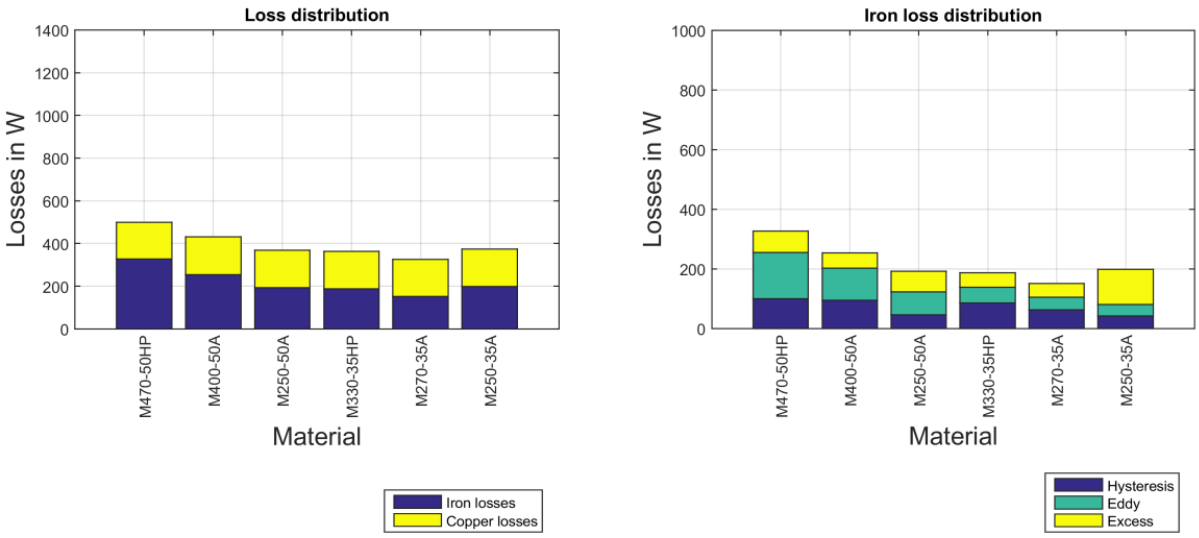

Figure 10: Integrated parameter reflecting the most likely loss components for WLTC Class 2 and machine 1 (PMSM delivery vehicle).

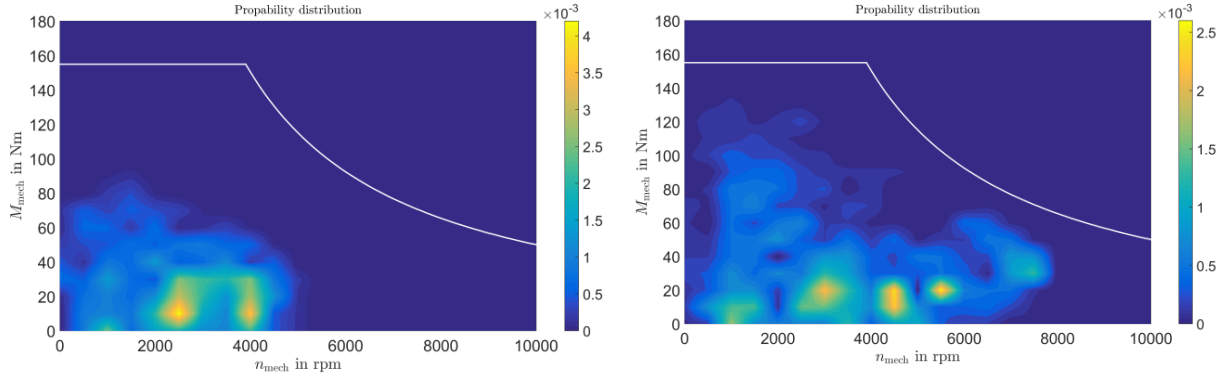

Figure 11: Probability distributions for WLTC Class 2 (left) and WLTC Class 3 (right) for machine 2 (PMSM midsize vehicle).

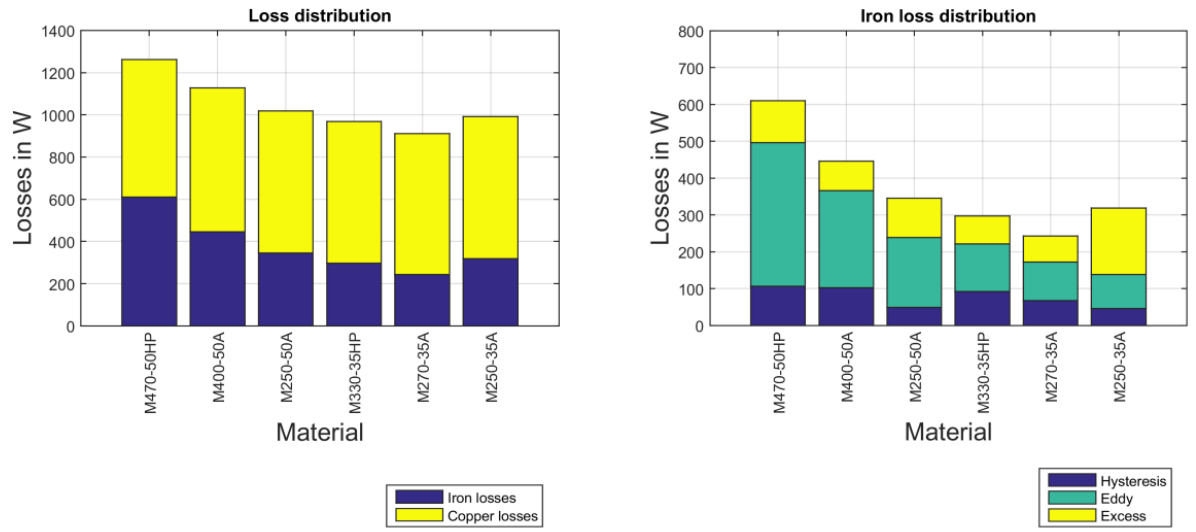

Figure 12: Integrated parameter reflecting the most likely loss components for WLTC Class 3 and machine 2 (PMSM midsize vehicle).

A high flux increases the ratio torque per current in the base frequency range, but in the field weakening area the flux has to be reduced by additional field weakening current, which compensates the advantage of materials with high polarization in driving cycles with an equal share of the base frequency and field weakening area.
High acceleration periods have a negligible impact on the integrated use of the machine. The vehicle accelerates and the operation point moves in the region of higher frequencies and lower torques, which results in short durations. As a result the iron losses define the overall material performance using PMSM. The order of material performance stays the same for both machines; just the distances are lower for machine 2, as a result of dominant copper losses.

In comparison to the PMSM the IM with squirrel cage rotor has a different method creating an excitation, which results in different operational characteristics discussed in section IV. This results in a different demand on material characteristics. As the induction machine has to create the excitation field by induction, the demand of high fluxes is increased.
As presented in figure 13 and 14 the results differ to the results presented for the PMSM. The increased copper losses are an outcome of additional losses in the squirrel cage to create the excitation field. The differences in the overall losses decrease. This results from different loss relations between copper and iron losses. M470-50HP has reduced copper losses but increased iron losses which decreases the distance to other materials. Comparing M250-50A with the thinner material M250-35A it has a higher sum of iron losses, which is a result of higher eddy current losses. The decrease of current demand compensates this effect with lower copper losses. Considering the operational characteristics of two different drive cycles, it makes no difference in the result. The advantage of higher torque per ampere ratio of materials with higher polarization can be used in the whole operation range. The proportion is still relevant. The higher share of iron losses for M470-50HP and M400-50A cannot be overcome by reducing the current demand. The relation between M250-50A and M250-35A has the right proportion to use cheaper material, which has other advantages in the manufacture process and thermal conductivity.

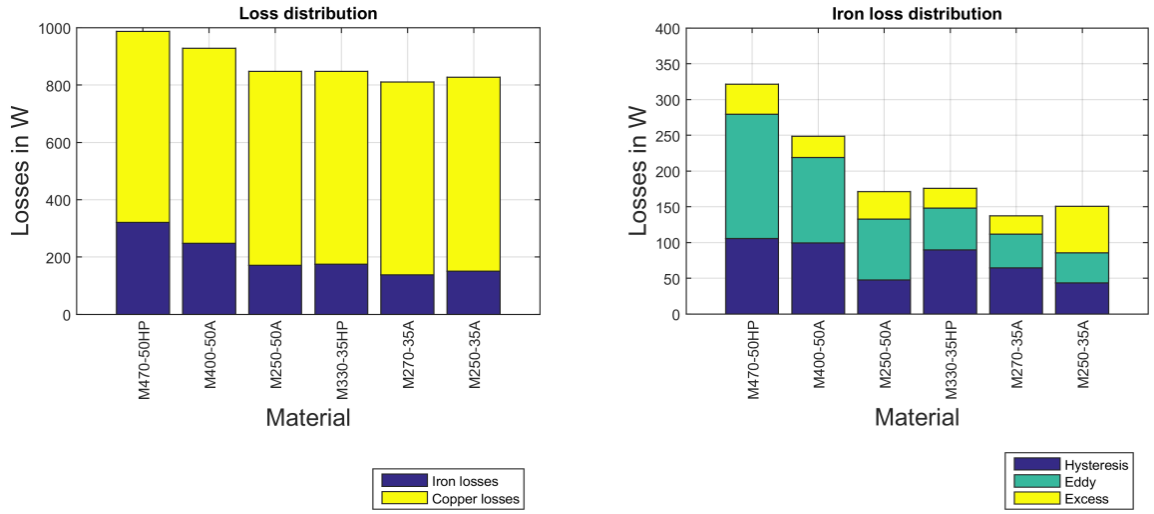

Figure 13: Integrated parameter reflecting the most likely loss components for WLTC Class 3 and machine 3 (IM minicar vehicle).

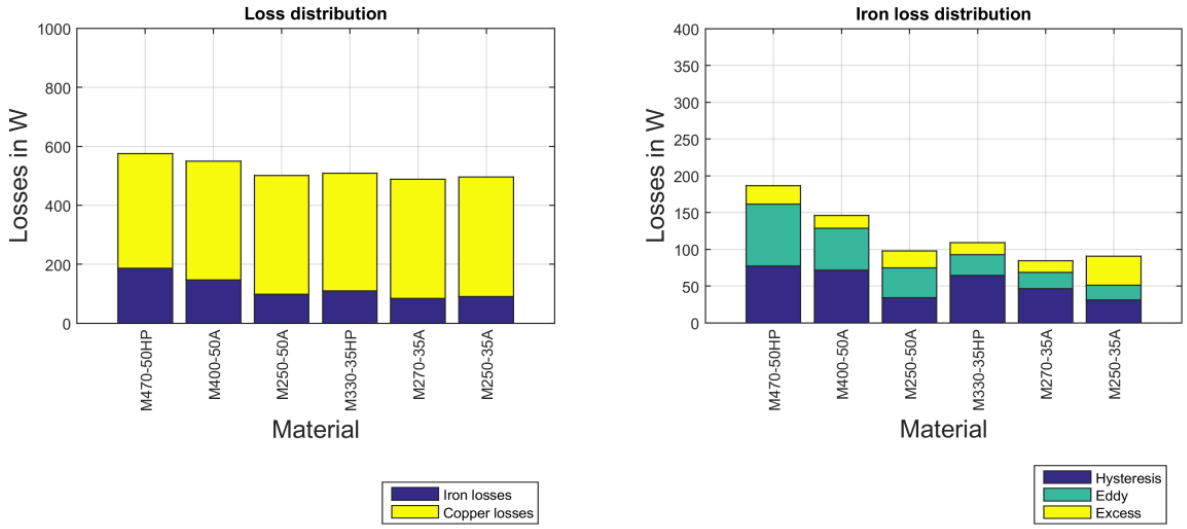

Figure 14: Integrated parameter reflecting the most likely loss components for WLTC Class 2 and machine 3 (IM minicar vehicle).

	Machine 1 (PMSM)			**Machine 2 (PMSM)**			**Machine 3 (IM)**		
Material	WLTC1	WLTC2	WLTC3	WLTC1	WLTC2	WLTC3	WLTC1	WLTC2	WLTC3
M250-35A	93.82	94.68	93.93	91.50	92.37	91.01	89.70	91.30	90.96
M270-35A	94.83	95.52	94.83	92.27	93.01	91.69	89.81	91.42	91.12
M330-35HP	94.07	94.92	94.27	91.58	92.46	91.20	89.46	91.09	90.76
M250-50A	93.95	94.72	93.69	91.50	92.29	90.79	89.67	91.21	90.76
M400-50A	92.69	93.71	92.74	90.30	91.33	89.91	88.86	90.45	89.97
M470-50HP	91.30	92.48	91.05	89.16	90.36	88.84	88.52	90.05	89.40

Table 4: Overall efficiency considering the probabilistic use of different machines and materials.

Table 4 summarizes the results comparing the efficiency of different machines applying different magnetic materials, weighted with the probabilistic distribution of different drive cycles. M270-35A shows the best performance for all machines and the studied drive cycles, although it has higher hysteresis and eddy current losses comparing with the supposed best material M250-35A. The low portion of excess losses, which results in lower sum of iron losses benefits in all driving situations.

VII. Conclusions

It is apparent from this paper that different machine topologies and the specific operation define the requirements on magnetic material characteristics. For application of electric traction drives in electrical vehicles, it is indispensable to consider the probabilistic distribution of operation areas. Electrical steel grades with increased magnetizability, so-called high permeability (HP) grades, or grades with very low losses do not lead to the highest efficiency and torque density by necessity. The advantages of high permeability grades leading to high fluxes which increase the torque

per ampere ratio and the machine utilization are harmful for field weakening. The design of high-saturation machines used in dynamic operation is less straightforward than standard industrial machines tailored to one specific operational point.
In order to evaluate the intricate coupling of magnetizability, iron losses and the application-specific requirements on torque and speed expressed in the driving cycle, this paper presents three different applications: a delivery vehicle, a midsize car and a minicar vehicle. These three different applications impose different requirements on the electrical steel grade. Two different PMSMs and one IM are employed as the most common machine topologies in electrical vehicle drive trains to evaluate the effect of different electrical steel grades, ranging from low-loss and high permeability grades to thicker and cheaper ones.
For PMSMs it has been shown that the advantage of high permeability, i.e., increased magnetic polarization, is beneficial in areas of high acceleration. There the higher torque per ampere ratio can reduce the Ohmic losses. This might be relevant for machines, which have a high probability of operating points in this area. The system response of the electrical vehicle leads to a direct increase of speed up to the desired area. In the field weakening area, i.e., at higher speeds, the additional flux needs to be reduced by additional currents leading to increased copper losses. This compensates the advantage of materials with high permeability. This is supported by the fact that the probability distribution of driving cycles of traction drives has a higher probability of operation in partial load areas, where iron losses are the dominant parameter to evaluate the material performance. The loss separation and localization where specific loss mechanisms are dominant define the requirements on the material selection. Detailed FE analysis has to be applied to ensure good accuracy of loss prediction. A comprehensive approach has shown that in case of IM the requirements on the magnetic material are different. As the induction machine has to create the excitation field by induction, the demand of high permeability is increased in the whole operational range. The probability of the machine operation defines the relevance of low loss distributions or high permeability of the magnetic materials.

References

[1] V. Ruuskanen, J. Nerg, J. Pyrhönen, S. Ruotsalainen, and R. Kennel, "Drive Cycle Analysis of a Permanent-Magnet Traction Motor Based on Magnetostatic Finite-Element Analysis," in *IEEE Transactions on Vehicular Technology*, vol. 64, no. 3, pp. 1249-1254, March 2015.

[2] S. Jacobs, D. Hectors, F. Henrotte, M. Hafner, M. H. Gracia, K. Hameyer, P. Goes, D. R. Romera, E. Attrazic, and S. Paolinelli, “Magnetic material optimization for hybrid vehicle PMSM drives,“ *Proc. Conf. EVS24*, 2009.

[3] P. H. Nguyen, E. Hoang and M. Gabsi, "Performance Synthesis of Permanent-Magnet Synchronous Machines During the Driving Cycle of a Hybrid Electric Vehicle," in *IEEE Transactions on Vehicular Technology*, vol. 60, no. 5, pp. 1991-1998, Jun 2011.

[4] M. Hombitzer, S. Steentjes, G. von Pfingsten, D. Franck, and Kay Hameyer, “Soft magnetic material modeling – The key to high power density electrical drives,” in *6th International Conference on Magnetism and Metallurgy - WMM 2014*, pages 442-455, Cardiff University, 2014.

[5] G. von Pfingsten, A. Ruf, S. Steentjes, M. Hombitzer, D. Franck, and Kay Hameyer, “Operating Point Resolved Loss Computation in Electrical Machines,” in *Archives of Electrical Engineering*, vol. 65(1), pp. 73-86, March 2016.

[6] J. de Santiago *et al*., "Electrical Motor Drivelines in Commercial All-Electric Vehicles: A Review," in *IEEE Transactions on Vehicular Technology*, vol. 61, no. 2, pp. 475-484, Feb. 2012.

[7] A. M. El-Refaie, "Motors/generators for traction/propulsion applications: A review," in *IEEE Vehicular Technology Magazine*, vol. 8, no. 1, pp. 90-99, March 2013.

[8] X. Liu; H. Chen; J. Zhao; A. Belahcen, "Research on the Performances and Parameters of Interior PMSM Used for Electric Vehicles," *in IEEE Transactions on Industrial Electronics* , vol. PP, no. 99, pp. 1-1, 2016.

[9] T. Finken, M. Felden and K. Hameyer, "Comparison and design of different electrical machine types regarding their applicability in hybrid electrical vehicles," *Electrical Machines, 2008. ICEM 2008. 18th International Conference on*, Vilamoura, 2008, pp. 1-5.

[10] Z. Yang, F. Shang, I. P. Brown and M. Krishnamurthy, "Comparative Study of Interior Permanent Magnet, Induction, and Switched Reluctance Motor Drives for EV and HEV Applications," in *IEEE Transactions on Transportation Electrification*, vol. 1, no. 3, pp. 245-254, Oct. 2015.

[11] G. Pellegrino, A. Vagati, B. Boazzo and P. Guglielmi, "Comparison of Induction and PM Synchronous Motor Drives for EV Application Including Design Examples," in *IEEE Transactions on Industry Applications*, vol. 48, no. 6, pp. 2322-2332, Nov.-Dec. 2012.

[12] D. G. Dorrell, A. M. Knight, L. Evans and M. Popescu, "Analysis and Design Techniques Applied to Hybrid Vehicle Drive Machines—Assessment of Alternative IPM and Induction Motor Topologies," in *IEEE Transactions on Industrial Electronics*, vol. 59, no. 10, pp. 3690-3699, Oct. 2012.

[13] T. Herold, D. Franck, E. Lange, and K. Hameyer, “Extension of a d-q model of a permanent magnet excited synchronous machine by including saturation, cross-coupling and slotting effects,” in *Electric Machines Drives Conference (IEMDC), 2011 IEEE International*, May 2011, pp. 1363–1367.

[14] F. Henrotte, G. Deliege, and K. Hameyer, “The eggshell approach for the computation of electromagnetic forces in 2D and 3D,” *COMPEL*, vol. 23, no. 4, pp. 996–1005, 2004.

[15] D. Kowal, P. Sergeant, L. Dupre, and H. Karmaker, "Comparison of Frequency and Time-Domain Iron and Magnet Loss Modeling Including PWM Harmonics in a PMSG for a Wind Energy Application," in *Energy Conversion, IEEE Transactions on* , vol.30, no.2, pp.476-486, June 2015.

[16] D. Lin, P. Zhou, W. Fu, Z. Badics, and Z. Cendes, "A dynamic core loss model for soft ferromagnetic and power ferrite materials in transient finite element analysis," in *Magnetics, IEEE Transactions on*, vol.40, no.2, pp.1318-1321, March 2004.

[17] Lammeraner J., Stafl M.; *Eddy Currents*; Iliffe Books Ltd. – London, 1966

[18] I. Podoleanu, J. Schneider, G. Müller, and K. Hameyer, “Software tool for the optimum material choice for induction machines,“ *Proc. Conf. OPTIM*, 2002.